Environmental Science & Technology

Article

Cite This: Environ. Sci. Technol. 2019, 53, 7136−7144

pubs.acs.org/est

Targeted Permeability Control in the Subsurface via Calcium Silicate Carbonation

Dan A. Plattenberger,[†] Florence T. Ling,[‡] Catherine A. Peters,[‡] and Andres F. Clarens*[,†]

[†]Engineering Systems and Environment, University of Virginia, Charlottesville, Virginia 22904, United States

[‡]Civil and Environmental Engineering, Princeton University, Princeton, New Jersey 08544, United States

Supporting Information

ABSTRACT: Efforts to develop safe and effective next-generation energy and carbon-storage technologies in the subsurface require novel means to control undesired fluid migration. Here we demonstrate that the carbonation of calcium silicates can produce reaction products that dramatically reduce the permeability of porous media and that are stable. Most calcium silicates react with CO_2 to form solid carbonates but some polymorphs (here, pseudowollastonite, $CaSiO_3$) can react to form a range of crystalline calcium silicate hydrates (CCSHs) at intermediate pH. High-pressure (1.1−15.5 MPa) column and batch experiments were conducted at a range of temperatures (75−150 °C) and reaction products were characterized using SEM-EDS and synchrotron μXRD and μXRF. Two characteristics of CCSH precipitation were observed, revealing unique properties for permeability control relative to carbonate precipitates. First, precipitation of CCSHs tends to occur on the surface of sand grains and into pore throats, indicating that small amounts of precipitation relative to the total pore volume can effectively block flow, compared to carbonates which precipitate uniformly throughout the pore space. Second, the precipitated CCSHs are more stable at low pH conditions, which may form more secure barriers to flow, compared to carbonates, which dissolve under acidic conditions.

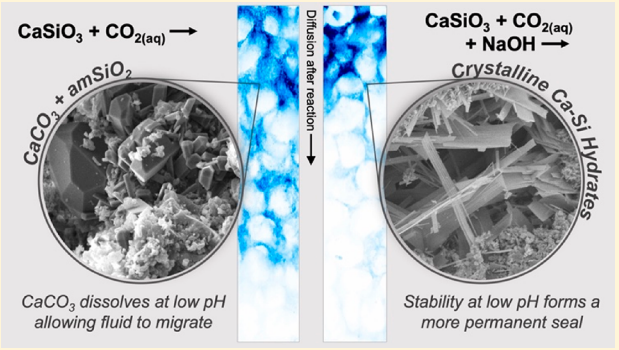

1. INTRODUCTION

The subsurface environment has traditionally been the source of most of our energy but a growing number of applications seek to use it to offset the environmental impacts of energy production.[1−3] Geologic carbon storage (GCS), enhanced geothermal energy (EGS), and compressed air energy storage leverage some of the unique characteristics of the subsurface (e.g., its size, temperature, and pressure) to store fluids or extract heat.[4−9] Because of the pressure gradients associated with fluid injection/production, strategies are needed to control fluid flow in target formations. Geophysical and/or geochemical alteration of the subsurface environment can create new and undesirable pathways for fluid migration.[10,11] In EGS, these are often referred to as thief zones, and undermine the economic viability of production. In GCS, leakage can contribute to groundwater contamination.[12] In addition, the influence that fluid migration has on induced seismicity remains problematic and difficult to predict.[13−16]

Strategies to control undesirable fluid migration are limited. The oil and gas industry has developed swelling polymers[17] and novel cementitious materials,[18] but they have limited utility in some subsurface applications because either the temperatures are too high or the leaks occur too far from the wellbore to reach.[19−21] Cements are also problematic because they are susceptible to degradation in acidic environments (like those present in CO_2 storage applications)[22−24] because they consist largely of calcium hydroxide $[Ca(OH)_2]$, which is soluble at low pH.[25] In addition, the high viscosity of cement limits its use to the wellbore vicinity and there, it does not often bind to metal casings or subsurface media, creating pathways that can grow over time.[21]

The use of mineralization reactions could sidestep some of the limitations associated with polymers or cement-based approaches. Recent work has demonstrated the viability of using microbially mediated calcite precipitation as a means of mitigating leakage in abandoned wells.[26,27] Other work has proposed the injection of a mineral silicate slurry followed by CO_2 to generate solid carbonates.[2] The most well-studied carbonates in these contexts are magnesium- or calcium-based minerals, which react via the following:

$$MSiO_{3(s)} + CO_{2(aq)} \rightarrow MCO_{3(s)} + SiO_{2(am)} \quad (1)$$

where M is the divalent cation. Magnesium-based carbonates prevail in basalt formations that are of interest from a CO_2-storage perspective[28] and calcium-based carbonates have faster reaction kinetics so they are common in laboratory experiments. The aqueous carbonation of wollastonite ($CaSiO_3$)

Received: February 4, 2019
Revised: April 22, 2019
Accepted: May 27, 2019
Published: May 28, 2019

DOI: 10.1021/acs.est.9b00707
Environ. Sci. Technol. 2019, 53, 7136−7144

under reservoir conditions (e.g., 90 °C, 25 MPa CO_2) produces porous, amorphous silica surrounding wollastonite cores, along with calcite, and sometimes, nanometer-scale Ca-phyllosilicates.[29] At 65 °C with ambient pressure of CO_2, Ashraf et al. reported similar products, including Ca-modified silica gels and Ca-carbonate/silica gel composites.[30] A common characteristic of solid carbonates is that they are sensitive to dissolution at low pH, meaning they could be an impermanent means of controlling flow:[14]

$$MCO_{3(s)} + 2H^+ \leftrightharpoons M^{2+} + CO_{2(aq)} + H_2O \quad (2)$$

In the mineral silicate system, the precipitation of these solid carbonates is dependent on the crystal structure of the parent silicates and the pH of the aqueous phase.[31] In chain-silicate minerals, preferential leaching of the cation allows the precipitation of solid carbonates in the presence of $CO_{2(aq)}$ and leaves a relatively unreactive porous silica network that condenses over time.[32] Our group recently reported that some mineral silicates can react with $CO_{2(aq)}$ to generate non-carbonate products.[31] Specifically, a ring-structured calcium silicate, pseudowollastonite ($CaSiO_3$) was shown to generate crystalline calcium silicate hydrates (CCSHs) in addition to Ca-carbonate when pH was increased at elevated temperature (150 °C) and moderate CO_2 concentration (0.18 M). The strained ring structure in pseudowollastonite allows for stoichiometric release of both Ca and dissolved Si, which can lead to the precipitation of various noncarbonate phases. We refer to these precipitates CCSHs to distinguish them from the amorphous calcium silicate hydrate phases that form in Portland cement, which are typically referred to as CSH gels. This nomenclature is also adapted from Richardson's work that summarized and modeled the calcium silicate hydrates that exist in nature and in engineered cements.[33] The composition of phases that form in the $CaO-SiO_2-(CO_2)-H_2O$ system is complex and highly variable, depending primarily on molar ratios of dissolved species, as shown in phase diagrams and schematics in Kaprálik et al.[34]

The goal of this work is to examine how the precipitation dynamics of carbonates and CCSHs impact fluid transport in porous media under natural or engineered conditions representative of the deep subsurface, which are expected to vary widely. For example, in basalt-based GCS, the relatively high pH of natural waters (9–11)[35] may facilitate CCSH precipitation, particularly in regions where the concentration of CO_2 is relatively low (e.g., the periphery of the CO_2 plume or in leakage locations). Likewise, pore solutions in concrete applications (e.g., wellbores) are often quite basic (approaching pH 13)[36] and could allow the precipitation of CCSHs. In saline-aquifer-based GCS, formation waters equilibrated with CO_2 are expected to be acidic, which would promote solid carbonate precipitation, followed by redissolution, unless the pH can be exogenously buffered enough to promote CCSH precipitation.

In particular, this work seeks to understand how permeability evolves over time in diffusion-limited carbonated silicate systems and is impacted by the presence of acid, which is common in many subsurface environments. These objectives were studied first via a series of sand column experiments that simulate porous media, in which pseudowollastonite was injected and then reacted with $CO_{2(aq)}$. Pseudowollastonite was selected based on our previous study that found it can generate a variety of carbonate and CCSHs, based on aqueous conditions.[31] The reacted columns were then characterized via synchrotron-based X-ray diffraction and X-ray fluorescence mapping as well as with electron microscope analyses which, together, allowed for spatial mapping of product phases under various conditions over time. Small powder batch experiments were also conducted to more fully characterize the reaction products and develop phenomenological relationships that might inform the deployment of this chemistry in the field.

2. EXPERIMENTAL MATERIALS AND METHODS

2.1. Sand Column Experiments. Pseudowollastonite powder (average powder diameter = 10.2 μm, SD = 8.4 μm, spongy/aggregated shape) was used as received from Sigma-Aldrich. NaOH (Sigma-Aldrich) was used to increase pH. Ottawa sand (500–841 μm fraction) was washed with 1 N HCl to remove surface impurities and rinsed with deionized water (18.2 MΩ cm, Millipore).

Sand columns, 1.59 cm in diameter and 5 cm in length, were produced by packing the washed and dried sand in 316 stainless-steel tubes that were capped at each end with stainless-steel washers and 250 μm stainless-steel mesh. After packing the tubes and oven drying, permeability and mass were measured for each column. Each was then placed in a press that held the columns in place while allowing fluid to be flowed through. Pseudowollastonite powder was suspended in deionized water (3 g/L) and injected into the columns at 10 MPa. During injection, a 20 μm porous disc was placed at the outlet end of each column to allow the passage of water and retention of pseudowollastonite. After injection, the columns were dried at 75 °C for 24 h and permeability and mass were again measured.

The bottom end of each column was pressed into a Teflon cap to seal it while the top end remained opened and they were then submerged upright in deionized water with either 0 M NaOH or 0.1 M NaOH in a 600 mL Teflon-lined stainless-steel pressure vessel, depicted in Figure 1. Hereafter, columns

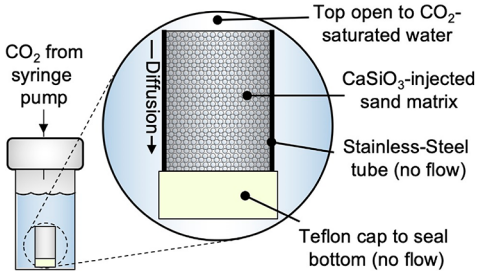

Figure 1. Sand columns were injected with a water–pseudowollastonite suspension and then submerged, upright, in a Teflon-lined, stainless-steel pressure vessel. CO_2 was injected into the headspace of the vessel with a syringe pump, where it equilibrated with the batch solution. CO_2 and other dissolved species could diffuse through the top (inlet) of the columns and react with the $CaSiO_3$.

reacted with only CO_2 are referred to as "CO_2 columns" and ones that were reacted with both CO_2 and NaOH are referred to as "CO_2 + NaOH columns". The experimental conditions are listed in Table 1. The water–CO_2 equilibrium pH was calculated with PHREEQC (V 2.18) using the PHREEQC database. The vessel was placed in an oven and heated while CO_2 (or N_2 for control columns) was injected into the headspace. We previously determined that total pressure has no observable impact on the reaction pathways of interest here.

DOI: 10.1021/acs.est.9b00707
Environ. Sci. Technol. 2019, 53, 7136–7144

Table 1. Experimental Conditions for Column Experiments

column number	reaction time (h)	temperature (°C)	[NaOH] (M)	pCO_2 (MPa)	[C] (M)[a]	batch pH[a]
1	24	90	0.1	1.1	0.22	6.16
2,3	48	90	0.1	1.1	0.22	6.16
4	96	90	0.1	1.1	0.22	6.16
5,6	168	90	0.1	1.1	0.22	6.16
7	16	150	0.1	1.1	0.19	6.65
8	24	150	0.1	1.1	0.19	6.65
9,10	48	150	0.1	1.1	0.19	6.65
11−13	96	150	0.1	1.1	0.19	6.65
14	108	150	0.1	1.1	0.19	6.65
15,16	288	150	0.1	1.1	0.19	6.65
17,18	447	150	0.1	1.1	0.19	6.65
19	495	150	0.1	1.1	0.19	6.65
20	12	150	0	1.1	0.09	3.94
21,22	48	150	0	1.1	0.09	3.94
23−26	96	150	0	1.1	0.09	3.94
27,28	168	150	0	1.1	0.09	3.94
29,30	447	150	0	1.1	0.09	3.94
31	495	150	0	1.1	0.09	3.94
32	24	150	0.1	0	0	10.49
33	96	150	0.1	0	0	10.49
34	24	150	0.1	3.4	0.38	6.16
35−41	72	150	0.1	3.4	0.38	6.16
42−47	72	150	0	3.4	0.29	3.68
48	24	150	0.1	15.5	1.35	5.52
49	24	150	0.1	3.4	0.28	3.65
50	0	N/A	N/A	N/A	N/A	N/A

[a]Initial batch pH, equilibrated with CO_2, calculated with PHREEQC

Instead, the partial pressure of CO_2 plays a crucial role. The columns were reacted for various times ranging from 12 to 495 h at temperatures ranging from 90 to 150 °C. While these temperatures are higher than those in most GCS applications, they were selected to accelerate chemical kinetics so that the experiments could be carried out over practical time scales. They were then dried at 75 °C and permeability and mass were again measured.

In select samples (columns 11−13, 19, 23−25, 31, and 50), the batch solutions were also doped with 15 mM strontium chloride hexahydrate, where Sr could diffuse into the columns and substitute for Ca in the precipitation of solid carbonates,[37] allowing for μXRF visualization of their precipitation dynamics. The Sr substitution method was required because Si and C are unobservable via μXRF and both the parent ($CaSiO_3$) and product ($CaCO_3$) minerals contained the same amount of Ca, rendering differentiation between the two otherwise challenging.

After the reaction periods and drying, the bottom ends of the same columns were again sealed and the columns were submerged upright in a 0.1 M NaBr solution, where the Br could diffuse into the column inlets and act as a visual complement to permeability with μXRF mapping (since no Br existed in the system prior to this step). To understand the temporal evolution of the reactions, 96 and 495 h columns were injected with epoxy and were sectioned along their length (1 mm thickness) for synchrotron μXRF and SEM-EDS. The remaining columns were thin-sectioned (to 30 μm) and mounted to Suprasil 2A quartz glass for synchrotron μXRD/μXRF.

To test the stability of the precipitates at different pH values, one set of experiments (numbers 35−47) that was reacted at 3.4 MPa CO_2, with or without NaOH, for 72 h were submerged in 1 M sodium acetate/acetic acid solutions[38] at pH values from 4 to 6 or in DI water and then flushed through with 20 mL DI water. They were then dried and the permeability and mass were measured.

2.2. Powder Batch Experiments. Small-scale powder batch experiments, were also conducted with the intention of isolating the effects of time and temperature on CCSH morphology and composition. The experimental setup for these experiments was described previously.[31] Briefly, 15 mg of pseudowollastonite powder was placed in 0.75 cm^3 Teflon boats with 1 g of sand and 0.5 mL of DI water, either with or without 0.1 M NaOH. The samples were reacted in a stainless-steel pressure vessel at 1.1 MPa CO_2 at a given experimental temperature and time. After each experiment, the samples were dried at 75 °C. One sample was dried in air at ambient temperature to compare to oven-dried samples. CCSHs were observed in the sample via SEM so we do not attribute their formation to the oven-drying process.

2.3. Air Permeability Measurements. For column experiments, permeability was determined by measuring the flow rate and pressure potential of air across the columns based on the technique of Tanikawa and Shimamoto[39] and is further described in the Supporting Information (SI).

2.4. Materials Characterization. Column samples were analyzed via synchrotron μXRD and/or μXRF at Argonne National Laboratory's Advanced Photon Source (13IDE). Further details about the beamline setup are described in Lanzirotti et al.[40] and in the SI. Spectral fitting of XRF data, XRF mapping, and local analyses of XRD data were performed in Larch.[41]

DOI: 10.1021/acs.est.9b00707
Environ. Sci. Technol. 2019, 53, 7136−7144

A majority of the columns were cut open after reaction (whether epoxied or not) and observed under SEM-EDS (FEI Quanta LV200). For powder batch systems, SEM-EDS was used to analyze all samples and select samples were analyzed with TEM/SAED (FEI Titan).

To analyze Si:Ca ratios and infer minerology for small powder batch experiments, CCSHs that formed over various reaction periods were observed under SEM by scanning across sample stubs and locating as many CCSH clusters as possible. When clusters were located, EDS spectra were acquired for individual plates and the silicon-to-calcium ratios were recorded.

3. RESULTS

3.1. Precipitates and Their Impact on Sand Column Permeability. Two broad classes of precipitate morphologies were observed in the experimental and control columns as shown in the SEM micrographs presented in Figure 2. The reaction products observed in columns injected with pseudowollastonite and reacted only in the presence of CO_2 are presented in Figure 2a. Under these conditions the reaction with pseudowollastonite follows eq 1 and yields Ca-carbonate and amorphous SiO_2, primarily. In contrast, the reaction products observed in columns reacted in the presence of CO_2 + NaOH are presented in Figure 2b,c.

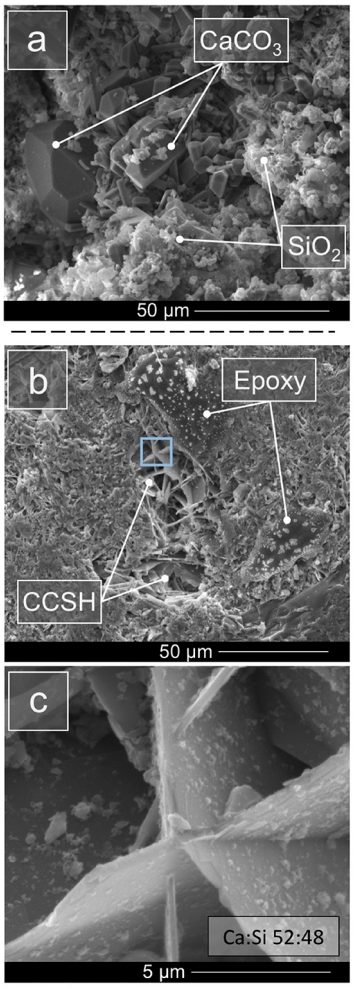

Figure 2. (a) Representative calcium carbonate and amorphous silica morphologies, which result from aqueous pseudowollastonite carbonation with unmodified pH (no NaOH added) at 1.1 MPa P_{CO2}. (b,c) An example of CCSH morphology from an epoxied and sectioned column, resulting from aqueous pseudowollastonite carbonation with elevated pH (0.1 M NaOH). Sheet-like morphology was the predominantly observed for CCSHs in the columns.

The two types of precipitates shown in Figure 2 had distinctly different impacts on permeability over time, as shown in Figure 3. While decreases in permeability were observed in all columns, there were order-of-magnitude differences for those containing carbonates alone and those containing CCSHs. The results in Figure 3 are plotted as a permeability reduction relative to the permeability of columns prior to reaction, which was generally on the order of 10−100 mD. Results from CO_2 columns, presented in blue, show that permeability reduction from the precipitation of carbonates was limited to a maximum 1.16 orders of magnitude (from 37 to 2.5 mD) in the 495 h reaction time at 150 °C (columns 20−31) and permeability reduction slowed after 168 h of reaction. In contrast, the CO_2 + NaOH columns (presented in orange, columns 7−19) exhibited continuously decreasing permeability, with a maximum reduction of 2.83 orders of magnitude (from 163 to 0.24 mD) after 495 h of exposure. CO_2 + NaOH columns that were reacted at 90 °C (to determine whether CCSHs could form and impact permeability at a range of temperatures, columns 1−6) follow a similar trend in permeability. For example, at 96 h, the 90 °C column experienced a decrease in permeability of 0.78 orders of magnitude while the 150 °C columns experienced an average 0.75 orders of magnitude decrease. In control columns (32 and 33), where N_2 was used instead of CO_2, there was nearly no change in permeability (in fact, a slight increase from 69 to 99 mD at 96 h of reaction) and there were no observed reaction products.

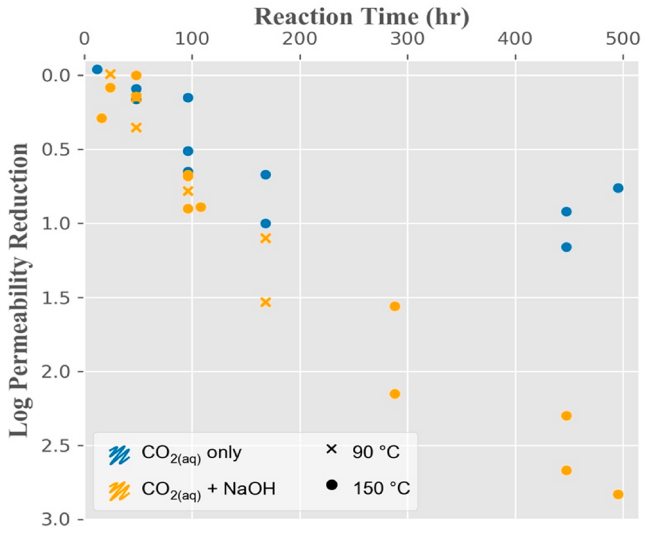

Figure 3. Log reduction of permeability for columns reacted in (blue) CO_2 only and (orange) CO_2 + NaOH as a function of reaction time.

3.2. μXRF Mapping of Precipitation and Diffusivity. Synchrotron μXRF maps of columns 31 (CO_2), 19 (CO_2 + NaOH), and 50 (unreacted control) are presented in Figure 4. Each map was collected from the column's inlet (top) to a depth of 8 mm, over a width of 1.5 mm. Strontium substituted for Ca in aragonite, as expected, which was the principle carbonate that precipitated under these conditions (from

DOI: 10.1021/acs.est.9b00707
Environ. Sci. Technol. 2019, 53, 7136−7144

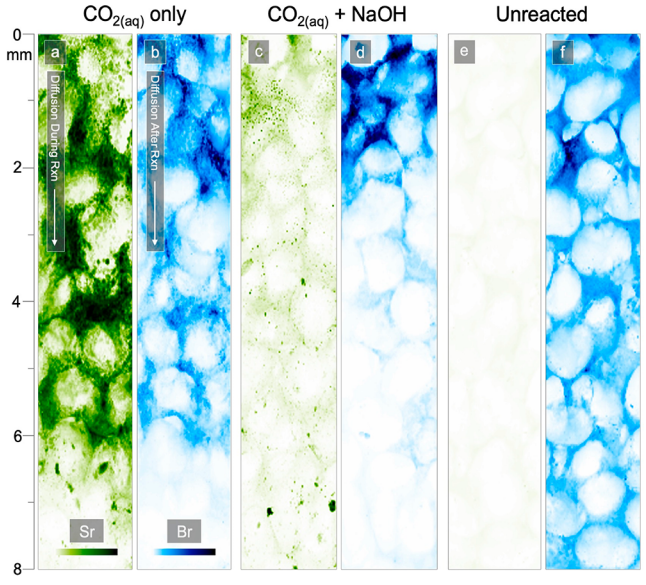

Figure 4. Micro-XRF maps of (green) Sr and (blue) Br for the inlet 8 mm of columns reacted for 495 h in (a,b) CO_2 only and (c,d) CO_2 + NaOH compared to (e,f) an unreacted column. Dissolved Sr was present during the reaction period and appeared to coprecipitate with Ca in Ca-carbonate. Columns were submerged, upright, in a Br solution after the reaction period to visualize diffusivity of the columns, as a complement to permeability measurements. Each Sr map shares a common color scale. Likewise, each Br map shares a common color scale. The intensities shown in these maps are proportional to element concentrations.

μXRD analyses). In contrast, Sr did not substitute to a large extent in the CCSHs so the green Sr maps in Figure 4 show the differences in carbonate precipitation between the columns.

In the CO_2 column, an abundance of Sr was observed in the first 7 mm (Figure 4a), indicating a large quantity of solid carbonate precipitation. The Br maps illustrate the relative diffusivity of water into the columns following the reaction period. The Br front (Figure 4b) nearly mirrored the Sr front, confirming that precipitates play an important role in controlling permeability. The permeability of the CO_2 column decreased from 87 mD to 15 mD during the reaction period. In contrast, the maps of the CO_2 + NaOH column show Sr at relatively lower concentrations than in the CO_2 column, indicating less precipitation of solid carbonates (Figure 4c) and bromine (Figure 4d) was generally limited to the first 2−3 mm of the column but at high concentrations relative to the inlet of the CO_2 column. The permeability of the column decreased from 163 mD to 0.24 mD during the reaction period. It should also be noted that even though the columns were approximately 50 mm in length, the vast majority of precipitation and physical change occurred within the first ∼5−8 mm at 495 h. Permeability measurements assume a homogeneous medium throughout the entire length of the column and assuming the change in permeability is due primarily to the reacted regions, the permeabilities of the reacted zones are likely significantly lower than reported. The final column shown in Figure 4 is a control that was unreacted (and therefore never exposed to Sr) so μXRF mapping shows no observable quantities of Sr (Figure 4e) and the bromine front exceeded 8 mm (Figure 4f). The permeability of that column was 141 mD.

3.3. Precipitation Locations within Pores. Micro-XRF and SEM-EDS analyses of thin-sectioned columns suggest that the mechanisms that drive the reductions in permeability in the CO_2 and the CO_2 + NaOH columns are observably different. In the CO_2 columns, solid carbonates precipitated randomly, without any preferred location within a given pore (e.g., in the pore body, along sand grain surfaces, or in pore throats; Figure 5a), which was expected from previous work in carbonate precipitation.[42] In contrast, the CCSHs that formed in the CO_2 + NaOH columns tended to form preferentially along the edges of sand grains, including in pore throats, which left a considerable amount of the pore body relatively open. A representative cross-section of a pore is shown in Figure 5b where the dark region, filled with epoxy, indicates a large open pore body (also evident from μXRF in Figure 4d). EDS maps of the region (Figure 5c,d) show that the CCSHs are Si-rich but also contain Ca. The tendency for these CCSHs to nucleate and grow on sand grain surfaces, including where grains are close to one another, indicates that pore throats are filled relatively quickly, potentially leading to dramatic decreases in permeability.

3.4. Temporal Evolution of Reaction Fronts. The reaction fronts in the CO_2 and CO_2 + NaOH columns evolved differently over time. After reacting for 96 h, the carbonation front in CO_2 columns penetrated approximately 3 mm into the column and was uniformly distributed across the inlet of the column (Figure 6a). Bromine was abundant and exceeded 8 mm, indicating that water was able to diffuse though this column (the first 5 mm are shown in Figure 6b while a 16 mm Br map is shown in the SI). After reaction for 495 h, the Sr front advanced to nearly 8 mm but was nonuniformly distributed normal to the direction of diffusion (Figure 6c). In some areas near the inlet, both Sr and Ca concentrations (Ca not shown) were low, suggesting that the carbonate that precipitated in this region dissolved in accordance with eq 2, leaving large, open spaces (see SI) allowing Br to diffuse to a depth >8 mm (Figure 6d). The carbonate redissolution could explain why the permeability in the CO_2 columns did not continue to decrease over longer durations.

In contrast, the reaction front of CO_2 + NaOH columns never exceeded ∼3 mm, regardless of reaction time. This could explain why the permeability in these columns continued to drop over time. SEM analyses suggest that the large redissolved regions did not exist in the CO_2 + NaOH columns.

3.5. Effects of Ion Concentrations on Precipitation Products and Permeability. To explore the effect of CO_2 on CCSH formation in columns, the partial pressure of CO_2 was varied in several experiments. When the P_{CO2} was increased to 3.4 MPa for 24 h (column 34, 0.1 M NaOH), an abundance of CCSHs and Ca-carbonate were observed near the inlet of the column. The permeability of the column decreased by 1.02 orders of magnitude (47.8 to 4.6 mD) during reaction. At higher partial pressures of CO_2 (15.5 MPa, 24 h, column 48), the permeability after reaction was too low to measure in the laboratory, suggesting at least 3 orders of magnitude reduction (from 42.5 mD). Evaluation of the columns following reaction revealed that abundant CCSH and Ca-carbonate precipitates had formed in the first several mm of the column (see the SI).

These results suggest that the formation of CCSHs is pH dependent, which is consistent with studies of CSH gel in concrete. Interestingly, a few columns reacted without NaOH, at 3.4 MPa CO_2 for 72 h (numbers 42−47), also yielded some

DOI: 10.1021/acs.est.9b00707
Environ. Sci. Technol. 2019, 53, 7136−7144

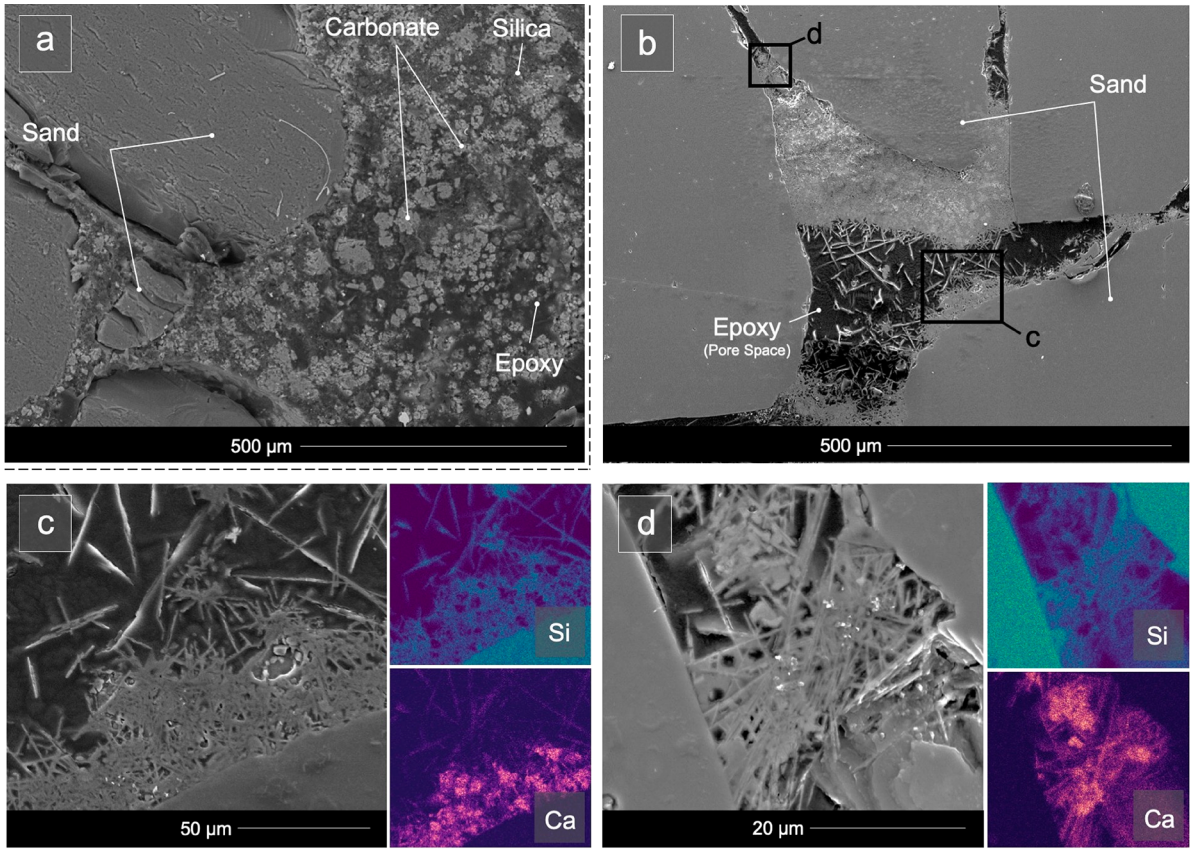

Figure 5. (a) SEM micrograph of a representative pore in a CO_2 column, where Ca-carbonate and amorphous silica precipitated throughout the pore body indiscriminately. (b) Compared to SEM cross-section of a representative pore in CO_2 + NaOH columns, showing a relatively open pore body but dense CCSH precipitation along sand grain edges and in the pore throats. (c,d) Inset EDS maps show that CCSHs in this pore appear to contain both calcium and silicon.

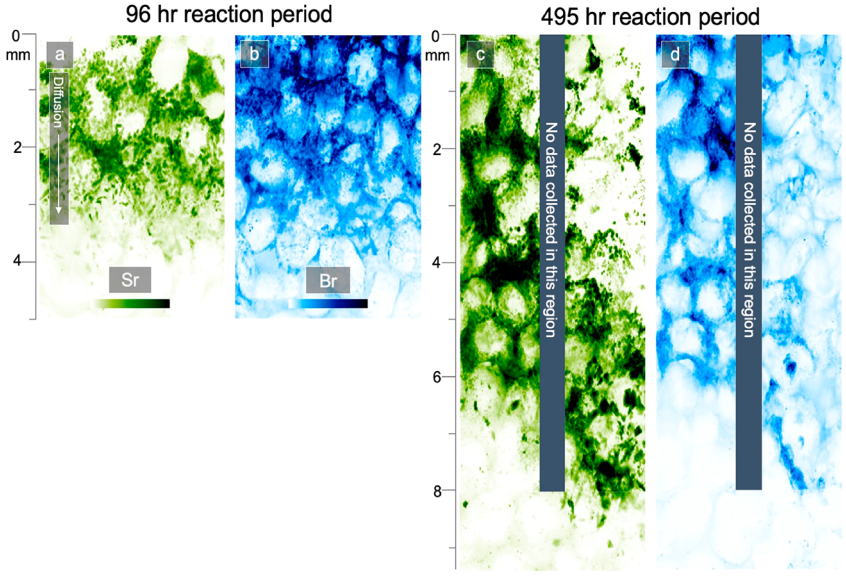

Figure 6. (a) Br and (b) Sr μXRF maps of 96 h CO_2 column experiments show a uniform carbonation front normal to the direction of diffusion. In contrast, at 495 h of reaction, the (c) Br and (d) Sr μXRF maps show a reaction front that is nonuniform and indicates redissolution of solid carbonates near the inlet of the column.

CCSHs, although at a much lower concentration than in columns containing NaOH. This result was unexpected, because we had not previously observed CCSH formation without NaOH present. Because of this result, we postulate that the concentration of dissolved carbon plays an important role in CCSH precipitation. Modeling (PHREEQC) suggests that in the 1.1 MPa experiments, the addition of NaOH increases the total dissolved carbon concentration in the batch

DOI: 10.1021/acs.est.9b00707
Environ. Sci. Technol. 2019, 53, 7136−7144

solution from 0.09 to 0.19 M. In the 3.4 MPa experiments, the dissolved carbon concentration is already high in both conditions due to the high pressure of CO_2 (0.38 and 0.29 M carbon, with and without NaOH, respectively). To ensure that the role of NaOH in this reaction mechanism was driven by the acid/base properties of OH^- and not Na^+ (since cations in solution have been shown to affect CO_2-induced dissolution of minerals),[43] one additional column (number 49) was reacted with 3.4 MPa CO_2 and 0.1 M NaCl rather than NaOH. The only products that were observed were Ca-carbonate and silica. In an analogous work in Mg carbonation, NaCl increased carbonate precipitation by increasing the Mg^{2+} dissolution rate, so the lack of CCSHs in this column could be due to that effect[44] or impacts from ionic strength but our previous experiments have shown that NaCl does not have a notable impact on CCSH formation when NaOH is present.

3.6. Stability of Reacted Columns under Acidic Conditions. To evaluate the long-term stability of these precipitated CCSHs, the permeability of two column types was evaluated following reaction for 72 h at a CO_2 pressure of 3.4 MPa (columns 35−47). The permeability of each sample was measured after a 16 h acid treatment in acetic acid/sodium acetate solutions[38] ranging from pH 4 to 6 (and a DI water control). As shown in Figure 7, in the CO_2 + NaOH columns, the permeability remained nearly constant after acid treatment, while in the CO_2 columns, permeability increased and approached the prereaction permeabilities. The pH 4.5 columns and the DI water columns were sectioned and observed under SEM, where it was apparent that CCSHs remained intact at approximately the same quantity (based on SEM observation) regardless of acid treatment while the Ca-carbonate in the pH 4.5 columns had largely been dissolved compared to the water control column (shown in the SI).

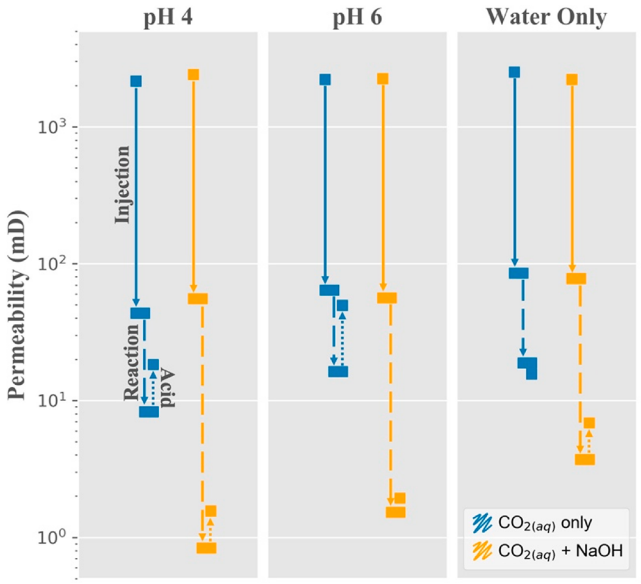

Figure 7. Permeabilities of (blue) CO_2 only columns and (orange) CO_2 + NaOH columns prior to $CaSiO_3$ injection, after injection, after the 72 h reaction period, and after 16 h acid diffusion at (top) pH 4 and (center) pH 6, and with only DI water diffusion (bottom).

3.7. Effects of Temperature on CCSH Precipitation. In our previously reported mechanism for precipitation of CCSHs, local concentrations of Ca and Si ions governed the stoichiometric ratios in the precipitates. In that case, a wide range of Ca and Si concentrations might be expected in the CCSHs because local ion concentrations are expected to vary considerably due to dissolution, precipitation, temperature, and chemical and pressure gradient effects. To extend that mechanism and study these reaction products, additional powder batch experiments were performed to better understand the effects that time and temperature have on these precipitates in the absence of the mass-transfer and heterogeneity effects that may exist in column experiments.

The first condition that was tested was the effect of temperature on CCSH formation. Experiments with 0.1 M NaOH and 1.1 MPa CO_2 were conducted for 24 h at 75, 90, 110, and 150 °C. At 75 and 90 °C (see the SI), Ca-carbonate precipitates predominated and even though CCSHs were present, they were small. At 110 °C, CCSHs were abundant, and there were no obvious differences from the 150 °C samples.

3.8. Effect of Time on CCSH Composition. An additional set of batch experiments at 150 °C was conducted for 24, 72, and 168 h to investigate the effect of time on CCSH composition. We did not observe a trend in Si/Ca ratios of the precipitated phases (Figure 8). It is clear that over the time scales tested here, a wide variety of mineral compositions are present within these CCSHs, ranging from Si-rich to Ca-rich.

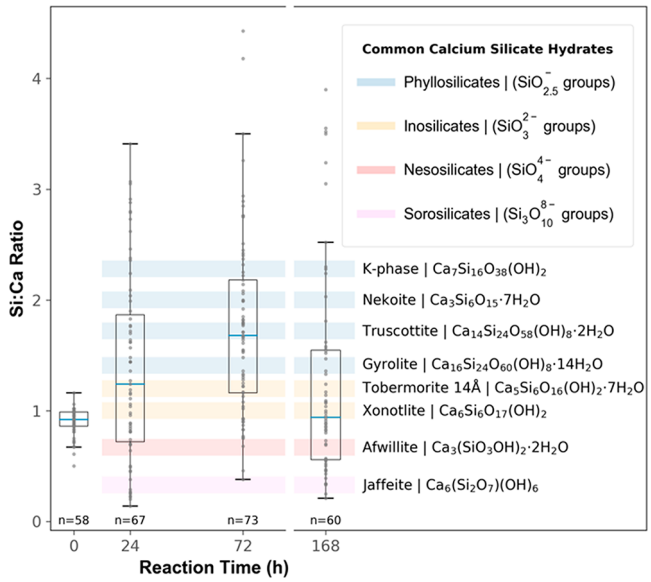

Figure 8. Silicon to Ca ratios of CCSH phases from powder batch experiments reacted in 0.1 M NaOH + 0.19 M CO_2 for 24, 72, and 168 h. The ratio for unreacted pseudowollastonite is also shown at 0 h. The Si/Ca ratios vary widely at all time periods and do not clearly seem to approach any particular ratio.

TEM-SAED analyses from 24 and 168 h experiments confirmed that the CCSHs were crystalline (i.e., bright diffraction spots) but each sample had a unique diffraction pattern and we were unable to definitively match any to known materials (see the SI). Approximately 90° symmetries were observed so only CCSHs that have at least partially orthogonal geometries are presented in Figure 8.

4. ENVIRONMENTAL IMPLICATIONS

The results presented here could enable new methods for controlling fluid flow in the subsurface. From a phenomeno-

DOI: 10.1021/acs.est.9b00707
Environ. Sci. Technol. 2019, 53, 7136−7144

logical perspective, the carbonation of calcium silicates that produce CCSHs effectively reduces the permeability of porous media to a greater extent than calcium silicates that produce only carbonates. From a mechanistic standpoint, we present evidence that the formation of these CCSHs is somewhat sensitive to pH but will form over a range of time, temperature, and P_{CO2} conditions. Taken together, these results inform an understanding needed to deploy this chemistry in the field, which may involve injecting mineral silicates in a pH-controlled slurry or tailoring the chemistry of injected fluids into formations.

The deliberate formation of CCSHs is an attractive means for blocking flow for a number of reasons. The apparent tendency for the CCSHs to precipitate on interfaces and in pore throats suggests that the reaction pathways identified here could be an efficient way to block flow in porous media. The stability of CCSHs relative to carbonates when exposed to acidic solutions suggests that CCSHs may be more effective at long-term stabilization and permeability control in geo-engineering applications.

Naturally, there will be challenges associated with using CCSHs to block flow in the subsurface. Understanding and, in some cases, engineering appropriate aqueous chemistry in complex and heterogeneous formations will require substantial efforts in field-scale observation and modeling. In some settings, such as EGS, CCSH-producing silicates might be injected. In other applications, such as GCS in basalts, having a detailed understanding of this chemistry could help explain fluid migration in some cases.

Finally, a number of aspects of CCSH formation are still poorly understood. For example, the role of CO_2 in these reactions has not yet been fully characterized. The formation of CCSHs does not appear to proceed without CO_2 yet none of the phases we have observed match known carbonate-containing calcium silicates, so future work could assess the specific role that CO_2 is playing in these reactions.

■ ASSOCIATED CONTENT

Supporting Information

The Supporting Information is available free of charge on the ACS Publications website at DOI: 10.1021/acs.est.9b00707.

Column setup and pseudowollastonite injection (Figure S1); permeability measurements; synchrotron μXRF/μXRD parameters; diffusion map for 96 hr CO_2 column (Figure S2); dissolving front (Figure S3); effect of CO_2 pressure on ccsh formation in CO_2 + NaOH columns (Figure S4); impacts of acid washing on carbonate and CCSH precipitates (Figure S5); effect of temperature on CCSH formation (Figure S6); TEM analyses of CCSH phases (Figure S7); XRD analysis of CCSH batch experiment (Figures S8 and S9); and additional references (PDF)

■ AUTHOR INFORMATION

Corresponding Author

*E-mail: andres@virginia.edu.

ORCID

Dan A. Plattenberger: 0000-0002-0775-2745
Catherine A. Peters: 0000-0003-2418-795X
Andres F. Clarens: 0000-0002-0606-9717

Notes

The authors declare no competing financial interest.

■ ACKNOWLEDGMENTS

Support for this work came from the United States Department of Energy National Energy Technology Laboratory (Grant DE-FE0026582) and the U.S. National Science Foundation (to AFC) (CBET-1134397 and CBET-1805075). Portions of this work were performed at GeoSoilEnviroCARS (The University of Chicago, Sector 13), Advanced Photon Source (APS), Argonne National Laboratory. GeoSoilEnviroCARS is supported by the National Science Foundation - Earth Sciences (EAR - 1634415) and Department of Energy-GeoSciences (DE-FG02-94ER14466). This research used resources of the Advanced Photon Source, a U.S. Department of Energy (DOE) Office of Science User Facility operated for the DOE Office of Science by Argonne National Laboratory under Contract No. DE-AC02-06CH11357.

■ REFERENCES

(1) Bruant, R. G., Jr.; Guswa, A. J.; Celia, M. A.; Peters, C. A. Safe Storage of CO2 in Deep Saline Aquifers. *Environ. Sci. Technol.* **2002**, *36* (11), 240A−245A.

(2) Tao, Z.; Fitts, J. P.; Clarens, A. F. Feasibility of Carbonation Reactions to Control Permeability in the Deep Subsurface. *Environ. Eng. Sci.* **2016**, *33* (10), 778−790.

(3) Clarens, A. F.; Peters, C. A. Mitigating Climate Change at the Carbon Water Nexus: A Call to Action for the Environmental Engineering Community. *Environ. Eng. Sci.* **2016**, *33* (10), 719−724.

(4) Atrens, A. D.; Gurgenci, H.; Rudolph, V. Economic Optimization of a CO $_2$ -Based EGS Power Plant. *Energy Fuels* **2011**, *25* (8), 3765−3775.

(5) Pruess, K. Enhanced Geothermal Systems (EGS) Using CO2 as Working Fluid—A Novel Approach for Generating Renewable Energy with Simultaneous Sequestration of Carbon. *Geothermics* **2006**, *35* (4), 351−367.

(6) Succar, S.; Williams, R. H. *Compressed Air Energy Storage: Theory Resources and Applications for Wind Power*; Princeton Environmental Institute, 2008.

(7) Dobson, P.; Kneafsey, T. J.; Blankenship, D.; Valladao, C.; Morris, J.; Knox, H.; Schwering, P.; White, M.; Doe, T.; Roggenthen, W.; et al. An Introduction to the EGS Collab Project. In *Transactions—Geothermal Resources Council*; Geothermal Resources Council, 2017; Vol. *41*, pp 837−849.

(8) Feng, R.; Liu, J.; Chen, S.; Bryant, S. Effect of Gas Compressibility on Permeability Measurement in Coalbed Methane Formations: Experimental Investigation and Flow Modeling. *Int. J. Coal Geol.* **2018**, *198*, 144−155.

(9) Jun, Y.-S.; Giammar, D. E.; Werth, C. J.; Dzombak, D. A. Environmental and Geochemical Aspects of Geologic Carbon Sequestration: A Special Issue. *Environ. Sci. Technol.* **2013**, *47* (1), 1−2.

(10) Ellis, B.; Peters, C.; Fitts, J.; Bromhal, G.; Mcintyre, D.; Warzinski, R.; Rosenbaum, E. Deterioration of a Fractured Carbonate Caprock Exposed to CO 2-Acidifi Ed Brine Fl Ow. *Greenhouse Gases: Sci. Technol.* **2011**, *1* (3), 248−260.

(11) Jun, Y.-S.; Giammar, D. E.; Werth, C. J. Impacts of Geochemical Reactions on Geologic Carbon Sequestration. *Environ. Sci. Technol.* **2013**, *47* (1), 3−8.

(12) Liang, B.; Clarens, A. F. Interactions Between Stratigraphy and Interfacial Properties on Flow and Trapping in Geologic Carbon Storage. *Water Resour. Res.* **2018**, *54* (1), 72−87.

(13) Vengosh, A.; Jackson, R. B.; Warner, N.; Darrah, T. H.; Kondash, A. A Critical Review of the Risks to Water Resources from Unconventional Shale Gas Development and Hydraulic Fracturing in the United States. *Environ. Sci. Technol.* **2014**, *48* (15), 8334−8348.

DOI: 10.1021/acs.est.9b00707
Environ. Sci. Technol. 2019, 53, 7136−7144

(14) Kutchko, B. G.; Strazisar, B. R.; Dzombak, D. A.; Lowry, G. V.; Thaulow, N. Degradation of Well Cement by CO2under Geologic Sequestration Conditions. *Environ. Sci. Technol.* **2007**, *41* (13), 4787−4792.
(15) Bauer, S.; Beyer, C.; Dethlefsen, F.; Dietrich, P.; Duttmann, R.; Ebert, M.; Feeser, V.; Görke, U.; Köber, R.; Kolditz, O.; Rabbel, W.; et al. Impacts of the Use of the Geological Subsurface for Energy Storage: An Investigation Concept. *Environ. Earth Sci.* **2013**, *70* (8), 3935−3943.
(16) Vidic, R. D.; Brantley, S. L.; Vandenbossche, J. M.; Yoxtheimer, D.; Abad, J. D. Impact of Shale Gas Development on Regional Water Quality. *Science* **2013**, *340* (6134), 1235009.
(17) Abidin, A. Z.; Puspasari, T.; Nugroho, W. A. Polymers for Enhanced Oil Recovery Technology. *Procedia Chem.* **2012**, *4*, 11−16.
(18) Mangadlao, J. D.; Cao, P.; Advincula, R. C. Smart Cements and Cement Additives for Oil and Gas Operations. *J. Pet. Sci. Eng.* **2015**, *129*, 63−76.
(19) Huang, Z.-Q.; Winterfeld, P. H.; Xiong, Y.; Wu, Y.-S.; Yao, J. Parallel Simulation of Fully-Coupled Thermal-Hydro-Mechanical Processes in CO2 Leakage through Fluid-Driven Fracture Zones. *Int. J. Greenhouse Gas Control* **2015**, *34*, 39−51.
(20) Gurevich, A. E.; Endres, B. L.; Robertson, J. O.; Chilingar, G. V. Gas Migration from Oil and Gas Fields and Associated Hazards. *J. Pet. Sci. Eng.* **1993**, *9* (3), 223−238.
(21) Gasda, S. E.; Bachu, S.; Celia, M. A. Spatial Characterization of the Location of Potentially Leaky Wells Penetrating a Deep Saline Aquifer in a Mature Sedimentary Basin. *Environ. Geol.* **2004**, *46* (6−7), 707−720.
(22) Mason, H. E.; Du Frane, W. L.; Walsh, S. D. C.; Dai, Z.; Charnvanichborikarn, S.; Carroll, S. A. Chemical and Mechanical Properties of Wellbore Cement Altered by CO_2 -Rich Brine Using a Multianalytical Approach. *Environ. Sci. Technol.* **2013**, *47* (3), 1745−1752.
(23) Newell, D. L.; Carey, J. W. Experimental Evaluation of Wellbore Integrity Along the Cement-Rock Boundary. *Environ. Sci. Technol.* **2013**, *47* (1), 276−282.
(24) Cheshire, M. C.; Stack, A. G.; Carey, J. W.; Anovitz, L. M.; Prisk, T. R.; Ilavsky, J. Wellbore Cement Porosity Evolution in Response to Mineral Alteration during CO_2 Flooding. *Environ. Sci. Technol.* **2017**, *51* (1), 692−698.
(25) Li, Q.; Lim, Y. M.; Flores, K. M.; Kranjc, K.; Jun, Y.-S. Chemical Reactions of Portland Cement with Aqueous CO 2 and Their Impacts on Cement's Mechanical Properties under Geologic CO 2 Sequestration Conditions. *Environ. Sci. Technol.* **2015**, *49* (10), 6335−6343.
(26) Cunningham, A. B.; Lauchnor, E.; Eldring, J.; Esposito, R.; Mitchell, A. C.; Gerlach, R.; Phillips, A. J.; Ebigbo, A.; Spangler, L. H. Abandoned Well CO_2 Leakage Mitigation Using Biologically Induced Mineralization: Current Progress and Future Directions. *Greenhouse Gases: Sci. Technol.* **2013**, *3* (1), 40−49.
(27) Hommel, J.; Lauchnor, E.; Phillips, A.; Gerlach, R.; Cunningham, A. B.; Helmig, R.; Ebigbo, A.; Class, H. A Revised Model for Microbially Induced Calcite Precipitation: Improvements and New Insights Based on Recent Experiments. *Water Resour. Res.* **2015**, *51* (5), 3695−3715.
(28) Giammar, D. E.; Wang, F.; Guo, B.; Surface, J. A.; Peters, C. A.; Conradi, M. S.; Hayes, S. E. Impacts of Diffusive Transport on Carbonate Mineral Formation from Magnesium Silicate-CO2-Water Reactions. *Environ. Sci. Technol.* **2014**, *48* (24), 14344−14351.
(29) Daval, D.; Martinez, I.; Guigner, J.-M.; Hellmann, R.; Corvisier, J.; Findling, N.; Dominici, C.; Goffe, B.; Guyot, F. Mechanism of Wollastonite Carbonation Deduced from Micro- to Nanometer Length Scale Observations. *Am. Mineral.* **2009**, *94* (11−12), 1707−1726.
(30) Ashraf, W.; Olek, J.; Jain, J. Microscopic Features of Non-Hydraulic Calcium Silicate Cement Paste and Mortar. *Cem. Concr. Res.* **2017**, *100*, 361−372.
(31) Plattenberger, D. A.; Ling, F. T.; Tao, Z.; Peters, C. A.; Clarens, A. F. Calcium Silicate Crystal Structure Impacts Reactivity with CO_2 and Precipitate Chemistry. *Environ. Sci. Technol. Lett.* **2018**, *5* (9), 558−563.
(32) Casey, W. H.; Westrich, H. R.; Banfield, J. F.; Ferruzzi, G.; Arnold, G. W. Leaching and Reconstruction at the Surfaces of Dissolving Chain-Silicate Minerals. *Nature* **1993**, *366* (6452), 253−256.
(33) Richardson, I. G. The Calcium Silicate Hydrates. *Cem. Concr. Res.* **2008**, *38* (2), 137−158.
(34) Kaprálik, I.; Števula, L.; Petrovič, J.; Hanic, F. Study of the System CaO-SiO2-CO2-H2O in Relation to Scawtite under Hydrothermal Conditions. *Cem. Concr. Res.* **1984**, *14* (6), 866−872.
(35) Gislason, S. R.; Wolff-Boenisch, D.; Stefansson, A.; Oelkers, E. H.; Gunnlaugsson, E.; Sigurdardottir, H.; Sigfusson, B.; Broecker, W. S.; Matter, J. M.; Stute, M.; Axelsson, G. Mineral Sequestration of Carbon Dioxide in Basalt: A Pre-Injection Overview of the CarbFix Project. *Int. J. Greenhouse Gas Control* **2010**, *4* (3), 537−545.
(36) Huet, B.; L'Hostis, V.; Miserque, F.; Idrissi, H. Electrochemical Behavior of Mild Steel in Concrete: Influence of PH and Carbonate Content of Concrete Pore Solution. *Electrochim. Acta* **2005**, *51* (1), 172−180.
(37) Lauchnor, E. G.; Schultz, L. N.; Bugni, S.; Mitchell, A. C.; Cunningham, A. B.; Gerlach, R. Bacterially Induced Calcium Carbonate Precipitation and Strontium Coprecipitation in a Porous Media Flow System. *Environ. Sci. Technol.* **2013**, *47* (3), 1557−1564.
(38) Han, F. X.; Banin, A. Selective Sequential Dissolution Techniques for Trace Metals in Arid-zone Soils: The Carbonate Dissolution Step. *Commun. Soil Sci. Plant Anal.* **1995**, *26* (3−4), 553−576.
(39) Tanikawa, W.; Shimamoto, T. Comparison of Klinkenberg-Corrected Gas Permeability and Water Permeability in Sedimentary Rocks. *Int. J. Rock Mech. Min. Sci.* **2009**, *46* (2), 229−238.
(40) Lanzirotti, A.; Newville, M.; Manoukian, L.; Lange, K. High-Speed, Coupled Micro-Beam XRD/XRF/XAFS Mapping at GSE-CARS: APS Beamline 13-ID-E. *Clay Clay Miner* **2016**, *22*, 53−64.
(41) Newville, M. Larch: An Analysis Package for XAFS and Related Spectroscopies. *J. Phys.: Conf. Ser.* **2013**, *430* (1), 012007.
(42) Zhang, C.; Dehoff, K.; Hess, N.; Oostrom, M.; Wietsma, T. W.; Valocchi, A. J.; Fouke, B. W.; Werth, C. J. Pore-Scale Study of Transverse Mixing Induced $CaCO_3$ Precipitation and Permeability Reduction in a Model Subsurface Sedimentary System. *Environ. Sci. Technol.* **2010**, *44* (20), 7833−7838.
(43) Min, Y.; Kim, D.; Jun, Y.-S. Effects of Na^+ and K^+ Exchange in Interlayers on Biotite Dissolution under High-Temperature and High-CO_2 -Pressure Conditions. *Environ. Sci. Technol.* **2018**, *52* (22), 13638−13646.
(44) O'Connor, W. K.; Dahlin, D. C.; Rush, G. E.; Gerdemann, S. J.; Penner, L. R.; Nilsen, D. N. *Aqueous Mineral Carbonation: Mineral Availability, Pretreatment, Reaction Parametrics, and Process Studies*; 2005. DOI: 10.13140/RG.2.2.23658.31684.

DOI: 10.1021/acs.est.9b00707
Environ. Sci. Technol. 2019, 53, 7136−7144